Speed-Sensorless DFIG Wind Drive Based on DTC Using Sliding Mode Rotor Flux Observer

Jihène Ben Alaya*‡, Adel Khedher**, Mohamed Faouzi Mimouni*

*RME, Monastir Engineering School (ENIM)

**RELEV, Sousse Engineering School (ENISO)

bnajihene@yahoo.fr, adel_kheder@yahoo.fr , mfmimouni@enim.rnu.tn

‡ Corresponding Author; Jihène Ben Alaya, 23 rue des savants, Sousse, Tunisia, 4002, bnajihene@yahoo.fr

Received: 25.07.2012 Accepted: 14.09.2012

Abstract- In this paper, we present a grid-connected wind turbine equipped with double-fed induction generator directly connected to the grid in the stator side and interconnected via a power converter in the rotor side. The aim of this paper is to control the rotor side power converter via a speed sensorless direct torque control using a rotor flux observer based on the sliding mode method combined with the classical Lyapunov stability theory. The speed sensorless direct torque control seeks to provide a tracking of speed and rotor flux in spite of an unpredictable wind fluctuation. To control the grid side converter, a network voltage vector oriented control strategy is developed. The proposed strategies tested under parametric variations and different scenarios of wind speed disturbances, evaluate the system performances. Simulation results show that the wind variation has influence on the location of system operation mode. The introduction of the SMRFO allows a high fidelity, a good dynamic performance, an easier rotor flux regulation and a robustness against parameter variations.

Keywords- Wind Energy Converter System, DFIG, Sensorless Control, DTC, Flux Observer.

1. Introduction

In the aim to develop a quiet, efficient, and economical wind energy conversion systems (WECS) connected to the grid , different algorithm control applied to double-fed induction generator (DFIG) have been studied in the literature [1-5]. From these strategies, the field oriented control strategy (FOC) based on proportional-integral (PI) regulators [5] that has attracted much attention in the past few decades and the non linear vector control (NLVC) strategy based on lyopunov theorie [6]. But, those vector control strategies require accurate information of machine parameters which comes to compromise the robustness of the control device. After this, the direct control techniques namely the direct torque control (DTC) and the direct power control (DPC), based on two hysteresis comparators were proposed and compared to the vector control strategies. Direct control strategies of DFIG-based wind turbine systems have a simpler structure compared to the vector control strategies. Furthermore, DTC has a faster dynamic response due to the absence of the PI current controllers [2,7,8].

For the classical DTC applied to the DFIG, the rotor flux is estimated by the integration of the rotor voltage as described in [9]. At low frequency this integrator introduces saturation and noises, to overcome the problem, rotor flux and mechanical speed are measured as illustrated in [10]. In this paper, we have used a determinist observer based on the sliding mode principle to compute the rotor flux and the electromagnetic torque. The used sliding mode rotor flux observer (SMRFO) has been selected for its simplicity and robust stability properties. It presents an attractive choice for its being robust to parameter variations and external system noises [11,12].

On the other hand, sensorless operation is important for wind applications due to the need for low cost and high reliability particularly for wind turbines which are usually installed in harsh environment (including offshore and onshore wind farms). Thus, we have developed for a WECS based on a DFIG a speed sensorless direct torque control (SS_DTC) strategy based on a SMRFO combined with the classical Lyapunov stability theory.

This paper is organized as follows: In the second section we develop the model of the DFIG. In the third section, we present a rotor side converter control strategy based on the DTC principle. In the first step, we present the DTC principle and in the second step we estimate the rotor flux and the electromagnetic torque. The fourth section presents the SS_DTC. For this aim, we estimate firstly the DFIG speed and secondly we present the SMRFO. In the fifth section, grid side converter (GSC) model and network vector voltage oriented control (NVVOC) strategy are developed. Simulation works are presented and discussed in the sixth section. Finally, some concluding remarks end the paper.

2. Model of Dfig

In the stator reference frame (αs-βs), the mechanical/electrical energy conversion process is described by the equations of DFIG as follows [5,13]:

$$\begin{cases} v_{s\alpha}^{s} = R_s i_{s\alpha}^{s} + \dfrac{d\varphi_{s\alpha}^{s}}{dt} \\ v_{s\beta}^{s} = R_s i_{s\beta}^{s} + \dfrac{d\varphi_{s\beta}^{s}}{dt} \\ v_{r\alpha}^{s} = R_r i_{r\alpha}^{s} + \dfrac{d\varphi_{r\alpha}^{s}}{dt} + \omega\varphi_{r\beta}^{s} \\ v_{r\beta}^{s} = R_r i_{r\beta}^{s} + \dfrac{d\varphi_{r\beta}^{s}}{dt} - \omega\varphi_{r\alpha}^{s} \\ (J_m + \dfrac{J_t}{m^2})\dfrac{d\omega}{dt} + f\omega = \dfrac{T_t}{G_b} - T_{em} \end{cases} \quad (1)$$

With:

The wind turbine torque is given by:

$$T_t = \frac{\rho\pi R_b^2 V_v^3}{2\Omega_t} C_p \quad (2)$$

In this study, for each wind speed the rotational speed is varied to track the maximum power curve [5,14,15] as shown in figure (1).

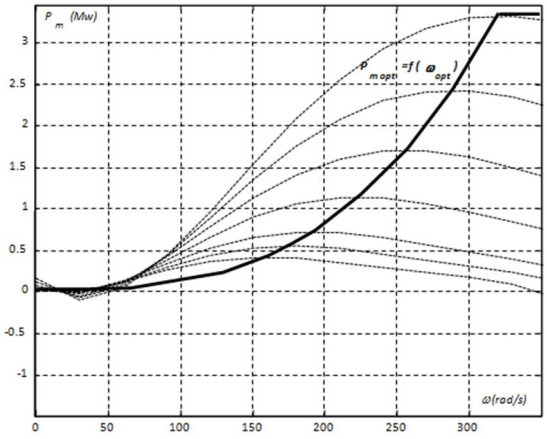

Fig. 1. Mechanical turbine power variations Versus speed and optimal-speed

The optimum power produced by the turbine vs. electrical speed is given by the following *Gaussian* equation:

$$\begin{cases} P_t = 5.24310^6 e^{-(\frac{\omega - 453.1}{187.2})^2} & \text{if} \quad V_v < 25\text{m/s} \\ P_t = 3.4MW & \text{if} \quad V_v \geq 25\text{m/s} \end{cases} \quad (3)$$

The electromagnetic torque developed by a DFIG, is expressed using stator and rotor flux vectors as follows:

$$T_{em} = \frac{3}{2}\frac{n_p M}{\sigma L_s L_r} \Im m(\varphi_{s\alpha\beta}^{*} \varphi_{r\alpha\beta}) \quad (4)$$

The stator and rotor flux can be expressed as follows:

$$\begin{cases} \varphi_{s\alpha\beta}^{s} = L_s i_{s\alpha\beta}^{s} + M i_{r\alpha\beta}^{s} \\ \varphi_{r\alpha\beta}^{s} = L_r i_{r\alpha\beta}^{r} e^{j\theta_m} + M i_{s\alpha\beta}^{s} \end{cases} \quad (5)$$

The stator and rotor currents vectors can be expressed as follows:

$$\begin{cases} i_{s\alpha\beta}^{s} = \dfrac{1}{\sigma L_s}\varphi_{s\alpha\beta}^{s} - \dfrac{M}{\sigma L_s L_r}\varphi_{r\alpha\beta}^{s} \\ i_{r\alpha\beta}^{s} = \dfrac{1}{\sigma L_r}\varphi_{r\alpha\beta}^{s} - \dfrac{M}{\sigma L_s L_r}\varphi_{s\alpha\beta}^{s} \end{cases} \quad (6)$$

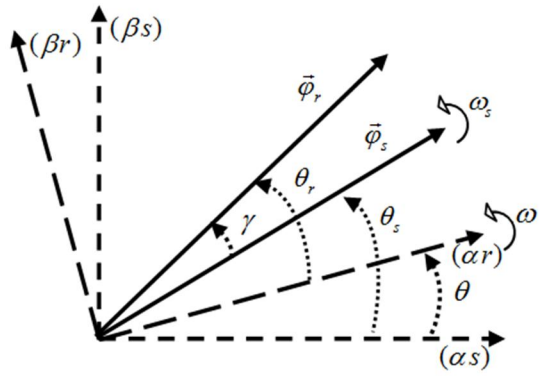

Fig. 2. Respective position of the references (αs,βs) and (αr,βr)

In a stationary reference frame (*αs-βs*), The DFIG electrical equations written in the state-space can be expressed as follows:

$$\frac{dX}{dt} = [A]X + [B]U \quad (7)$$

With:

$$X = \begin{bmatrix} i_{s\alpha} & i_{s\beta} & \varphi_{r\alpha} & \varphi_{r\beta} \end{bmatrix}^T$$

$$U = \begin{bmatrix} v_{s\alpha} & v_{s\beta} & v_{r\alpha} & v_{r\beta} \end{bmatrix}^T$$

$$[A]=\begin{bmatrix}[A_{11}] & [A_{12}]\\ [A_{21}] & [A_{22}]\end{bmatrix},\ [B]=\begin{bmatrix}[B_{11}] & [B_{12}]\\ [B_{21}] & [B_{22}]\end{bmatrix},$$

$$[A_{11}]=\begin{bmatrix}(\frac{-1}{\sigma\tau_S}-\frac{M^2}{\tau_r\sigma L_S L_r}) & 0\\ 0 & (\frac{-1}{\sigma\tau_S}-\frac{M^2}{\tau_r\sigma L_S L_r})\end{bmatrix},$$

$$[A_{12}]=\begin{bmatrix}\frac{M}{\tau_r\sigma L_S L_r} & \frac{\omega M}{\sigma L_S L_r}\\ -\frac{\omega M}{\sigma L_S L_r} & \frac{M}{\tau_r\sigma L_S L_r}\end{bmatrix},\ \mathrm{M}$$

$$[A_{21}]=\begin{bmatrix}\frac{M}{\tau_r} & 0\\ 0 & \frac{M}{\tau_r}\end{bmatrix},\ [A_{22}]=\begin{bmatrix}\frac{-1}{\tau_r} & -\omega\\ \omega & \frac{-1}{\tau_r}\end{bmatrix}$$

$$[B_{11}]=\begin{bmatrix}\frac{1}{\sigma L_S} & 0\\ 0 & \frac{1}{\sigma L_S}\end{bmatrix},\ [B_{12}]=\begin{bmatrix}-\frac{M}{\sigma L_S L_r} & 0\\ 0 & -\frac{M}{\sigma L_S L_r}\end{bmatrix}$$

$$[B_{21}]=[\Phi_{2,2}],\ [B_{22}]=[\mathrm{I}_{2,2}]$$

3. Classical Direct Torque Control

3.1. DTC Principle

The suggested control strategy is the Direct Torque Control (DTC) chosen for having a simpler structure compared to the Field Oriented Control strategy. Direct Torque Control is derived from the fact that, on the basis of the errors between the reference and the estimated values of torque and flux, it is possible to directly control the inverter states in order to reduce the torque and flux errors within the prefixed band limits. The DTC applied to control the DFIG is based on the same principle as for squirrel cage induction machine. The DTC technique selects the required rotor vector directly from the output of the torque and flux hysteresis comparators and the vector flux location [16]. The flux controller is based on a two level hysteresis comparator while the torque controller uses a three level hysteresis. Both controllers are characterized respectively by HF and HT hysteresis band illustrated by figure 3. In order to reduce the electromagnetic torque and flux ripples, the hysteresis bands width of both controllers (HT and HF) should be set to small values. In practice, those values are limited by the minimum switching sample period of the hardware board [10].

The rotor flux space evolution is divided into six sectors (Nsk).When rotor flux is in a sector (k), the control of flux and torque can be ensured by selecting one of the eight following voltage vectors:

$$\begin{cases}V_k=\sqrt{\frac{2}{3}}v_{dc}e^{j\frac{\pi}{3}(k-1)} & k\in[1,6]\\ V_0=V_7=0\end{cases} \quad (8)$$

The voltage vector selection is carried out according to the following table.

Table 1. Rotor voltage vector selection according to electromagnetic torque and flux errors.

Flux \ Torque		e_T		
		1	0	-1
e_φ	1	V_{k-1}	V_0 , V_7	V_{k+1}
	-1	V_{k-2}	V_0 , V_7	V_{k+2}

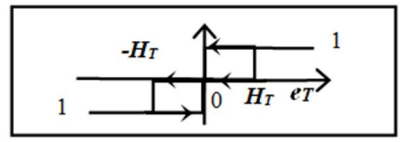

(a1)

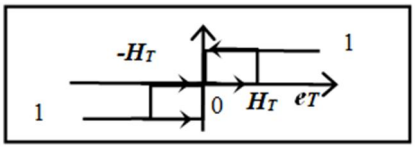

(a2)

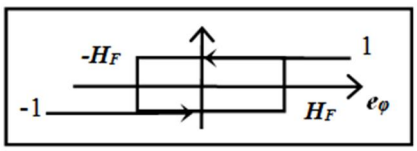

(b)

Fig. 3. (a) Electromagnetic torque hysteresis comparator: (a1) Subsynchronism, (a2) Hypersynchronism, (b) Rotor flux hysteresis comparator.

3.2. Flux and Electromagnetic Torque Estimation

In classical DTC applied to the DFIG, the estimated rotor flux is computed as follows:

$$\hat{\varphi}^s_{r\alpha\beta}=L_r i^s_{r\alpha\beta}+M i^s_{s\alpha\beta} \quad (9)$$

Rotor flux vector is computed from equation (5) and it represents the actual sector.

$$\angle\varphi_r=atg\left(\frac{\varphi_{r\beta}}{\varphi_{r\alpha}}\right) \quad (10)$$

The electromagnetic torque is computed from the measured currents and the machine parameters as follows:

$$\hat{T}em=\frac{3}{2}n_p M\,\Im m\left(i^*_{s\alpha\beta}i_{r\alpha\beta}\right) \quad (11)$$

The structure of the direct control is illustrated in figure (4).

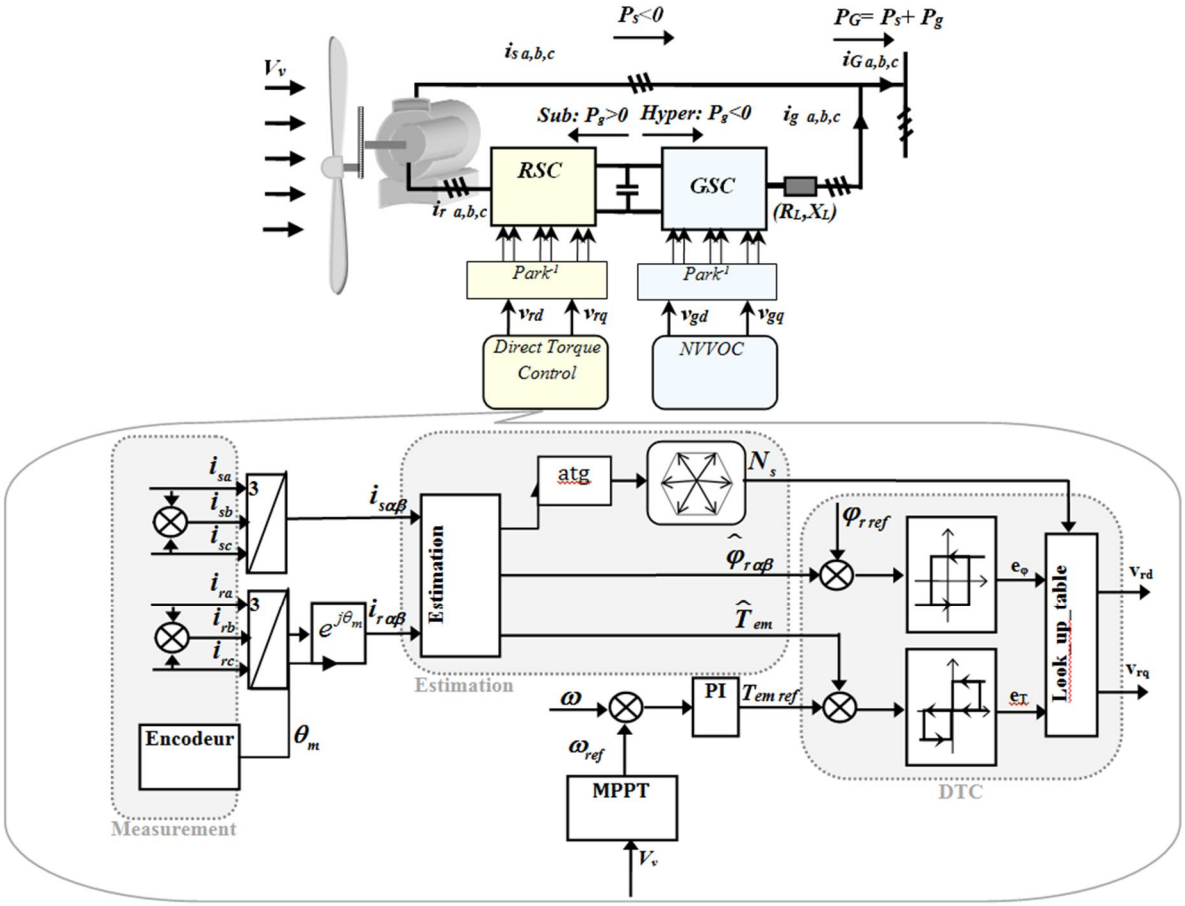

Fig. 4. Direct Torque Control structure applied to the proposed WECS

4. Speed Sensorless Dtc Development

The principal idea of this section is to develop firstly an approach to observe the rotor flux, using sliding mode technique combined with the classical *Lyapunov* stability theory, which will replace the estimated rotor flux considered in the DTC strategy treated in the previously section. Secondly, we propose the speed estimation via a SMRFO. The block diagram of figure (5) shows the basic idea of such approach.

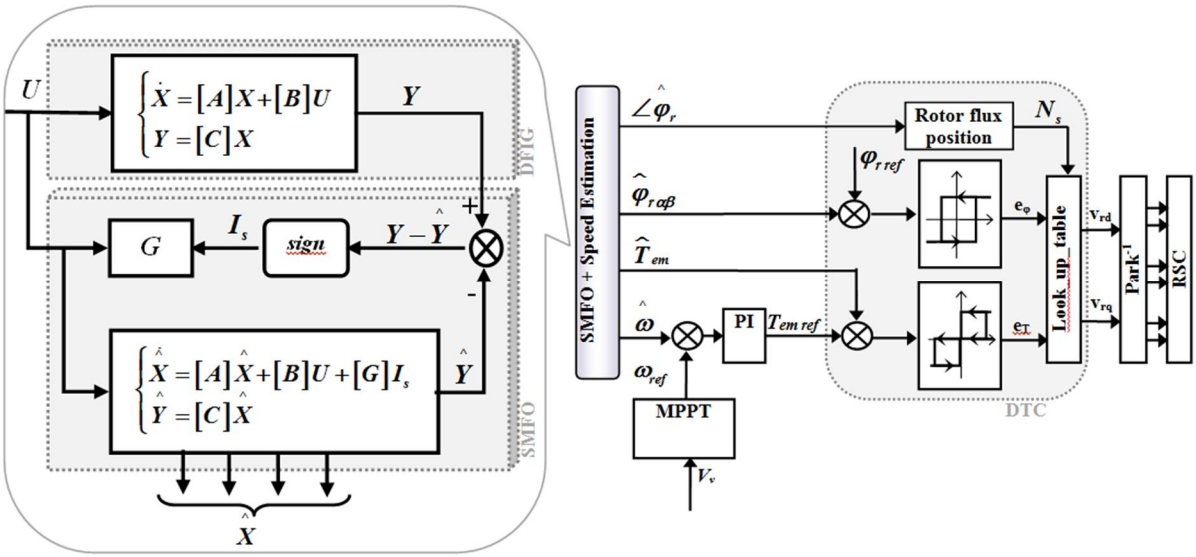

Fig. 5. Speed Sensorless DTC structure with SMRFO applied to a DFIG

4.1. Sliding Mode Rotor Flux Observer (SMRFO)

In this section, we use the state-space form using stator currents and rotor fluxes as expressed in the previous section. The idea is that the error between the actual and observed stator currents converges to zero, which guarantees the accuracy of the rotor flux observer. So, we define a sliding surface $S=[S_1\ S_2]^T$ as to converge to zero the two sliding variables (*i.e.* $S_1=0$, $S_2=0$). The sliding surface vector is given by:

$$S=\begin{bmatrix}S_1\\S_2\end{bmatrix}=D^{-1}\begin{bmatrix}i_{s\alpha}-i_{s\alpha e}\\i_{s\beta}-i_{s\beta e}\end{bmatrix} \tag{12}$$

With:

$$[D]=\begin{bmatrix}\dfrac{M}{\tau_r\sigma L_S L_r} & \dfrac{\omega_e M}{\sigma L_S L_r}\\ \dfrac{-\omega_e M}{\sigma L_S L_r} & \dfrac{M}{\tau_r\sigma L_S L_r}\end{bmatrix}=\begin{bmatrix}f_1 & f_2\\ f_3 & f_4\end{bmatrix} \tag{13}$$

If we denote as estimate of state vector , the sliding mode observer of the system is defined in the state-space as follows:

$$\frac{dX_e}{dt}=[A_e]X_e+[B]U+[G]I_S \tag{14}$$

With:

$$[A_e]=\begin{bmatrix}[A_{e11}] & [A_{e12}]\\ [A_{e21}] & [A_{e22}]\end{bmatrix},$$

$$[A_{e11}]=\begin{bmatrix}(\dfrac{-1}{\sigma\tau_S}-\dfrac{M^2}{\tau_r\sigma L_S L_r}) & 0\\ 0 & (\dfrac{-1}{\sigma\tau_S}-\dfrac{M^2}{\tau_r\sigma L_S L_r})\end{bmatrix},$$

$$[A_{e12}]=\begin{bmatrix}\dfrac{M}{\tau_r\sigma L_S L_r} & \dfrac{\omega_e M}{\sigma L_S L_r}\\ -\dfrac{\omega_e M}{\sigma L_S L_r} & \dfrac{M}{\tau_r\sigma L_S L_r}\end{bmatrix},$$

$$[A_{e21}]=\begin{bmatrix}\dfrac{M}{\tau_r} & 0\\ 0 & \dfrac{M}{\tau_r}\end{bmatrix},\ [A_{e22}]=\begin{bmatrix}\dfrac{-1}{\tau_r} & -\omega_e\\ \omega_e & \dfrac{-1}{\tau_r}\end{bmatrix}$$

[G]: The gain matrices for the observer, given by:

$$G=\begin{bmatrix}[G_i]\\ [G_\varphi]\end{bmatrix}=\begin{bmatrix}\begin{bmatrix}G_{11} & G_{12}\\ G_{21} & G_{22}\end{bmatrix}\\ \begin{bmatrix}G_{31} & G_{32}\\ G_{41} & G_{42}\end{bmatrix}\end{bmatrix}$$

The vector sign I_s is given by:

$$I_S=sign(S)=\begin{bmatrix}sign(S_1) & sign(S_2)\end{bmatrix}^T \tag{15}$$

It has been known that sliding mode techniques generate unexpected chattering that can degrade the control performance or can initiate high undesirable dynamic frequencies in the system [12]. One easy solution to avoid chattering is to replace the discontinued sign function by a continuous approximation with a high gain in the boundary layer like a saturation function.

$$sat(S_i)=\begin{cases}sign(S_i) & if\ \ |S_i|>\lambda_i\\ \dfrac{S_i}{\lambda_i} & if\ \ |S_i|\le\lambda_i\end{cases} \tag{16}$$

Where , is a smooth factor and *i=1,2.*

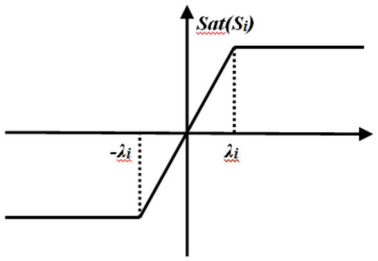

Fig. 6. Saturation function type

The proposed *Lyapunov's* candidate function is given by:

$$V=\frac{1}{2}S^T S \tag{17}$$

If we consider a high precision of the numerical treatment at the time of stator currents acquisition and that the dynamic of the observer is based on the exponential convergence of fluxes errors, the gain matrices for the observer can be expressed as follows:

$$\begin{aligned}G_i&=D\begin{bmatrix}\delta_1 & 0\\ 0 & \delta_2\end{bmatrix}\\ G_\varphi&=\begin{bmatrix}(f_3+q_1)\delta_1 & -\omega_e\delta_2\\ \omega_e\delta_1 & (f_3+q_2)\delta_2\end{bmatrix}\end{aligned} \tag{18}$$

Where the design parameters: q_1, q_2, δ_1 and δ_2 are positive constants.

The time derivative of the *Lyapunov* function given in (17) guarantee the system convergence toward the sliding manifold S, which are satisfied by the following condition:

$$\begin{cases}\delta_1\ge\left|e_3+\dfrac{f_1 f_3}{f_3^2+f_4^2}e_1-\dfrac{f_1 f_4}{f_3^2+f_4^2}e_2\right|\\ \delta_2\ge\left|e_4+\dfrac{f_1 f_4}{f_3^2+f_4^2}e_1+\dfrac{f_1 f_3}{f_3^2+f_4^2}e_2\right|\end{cases} \tag{19}$$

4.2. Speed Estimation

In order to achieve more economical control, speed sensor like tachometer or incremental encoder has been replaced by sensorless speed estimation. A sensorless control system allows to increase the strength and reliability and to decrease maintenance requirements of the system [17-19]. This is particularly important if the WECS is being used in a harsh and inaccessible environment.

So, to develop a sensorless speed control, we consider that the errors of the SMRFO converge to zero, in this condition, the observed fluxes can be written as follows:

$$\frac{d\varphi_{r\alpha\beta e}}{dt} = \frac{1}{\tau_r}(Mi_{s\alpha\beta e} - \varphi_{r\alpha\beta e}) - j\omega_e\varphi_{r\alpha\beta e} + v_{r\alpha\beta} \quad (20)$$

Hence, the rotational speed can be estimate as follows:

$$\omega_e = \frac{\left|\frac{d\varphi_{r\alpha\beta e}}{dt} + \frac{1}{\tau_r}\varphi_{r\alpha\beta e} - \frac{M}{\tau_r}i_{s\alpha\beta e} - v_{r\alpha\beta}\right|}{\left|j\varphi_{r\alpha\beta e}\right|} \quad (21)$$

5. Grid Side Converter Control

5.1. Grid Side Converter Model

The grid-side controller is a two-stage controller operating in a grid AC voltage reference frame. It controls the power flow exchange with the grid via the rotor. The GSC current output is determinated by Kirchhoff laws applied at the connection between the grid and the wind generator system.

$$\bar{v}g - \bar{v}_G = (R_L + jX_L)\,\bar{i}g + L_L\frac{d\bar{i}g}{dt} \quad (22)$$

With:

$$\begin{cases} \bar{v}G = \bar{v}s \\ \bar{i}G = \bar{i}s + \bar{i}g \end{cases}$$

The grid powers at the connection between the grid and the wind generator system are given by:

$$\begin{cases} P_G = P_S + P_g \\ Q_G = Q_S + Q_g \end{cases} \quad (23)$$

In the dc bus, the power P_{dc} is expressed as:

$$P_{dc} = Cv_{dc}\frac{dv_{dc}}{dt} = P_{em} - P_{js} - P_{jr} - P_S - P_g \quad (24)$$

With:

$$\begin{cases} P_{em} = T_{em}\omega_{méc} \\ P_{js} = \frac{3}{2}R_S(i_{s\alpha}^2 + i_{s\beta}^2) \\ P_{jr} = \frac{3}{2}R_r(i_{r\alpha}^2 + i_{r\beta}^2) \\ P_S = \frac{3}{2}\Re e(\bar{v}_s^{-s}\,\bar{i}_s^{s*}) \\ P_g = \frac{3}{2}\Re e(\bar{v}_G^{-s}\,\bar{i}g^{s*}) \end{cases}$$

5.2. Network Voltage Vector Oriented Control (NVVOC)

The network voltage vector oriented control (NVVOC) is adopted to control the GSC, which principle consists in orienting the d-axis Park frame (rotating at synchronous speed) according to the network voltage. This implies that:

$$\begin{cases} v_{Gd} = \left|\bar{v}_G\right| \\ v_{Gq} = 0 \end{cases} \quad (25)$$

Thus, the dynamics of the active and reactive powers become directly linked to the control of network currents components [5,6]. In these conditions, one can write:

$$\begin{cases} P_g = \frac{3}{2}v_G i_{gd} \\ Q_g = -\frac{3}{2}v_G i_{gq} \end{cases} \quad (26)$$

The proposed algorithm scheme is illustrated in figure (7).

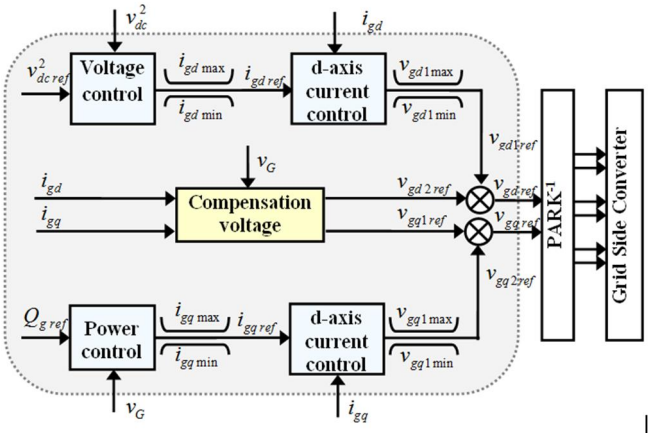

Fig. 7. NVVOC strategy diagram of GSC

6. Simulations results

Simulations results are made by using the real parameters of a wind turbine *AE43* and a DFIG rated at *660KW* and *690V*. The rotor flux reference is chosen equal to *3.1Wb* (nominal value). The wind turbine and the DFIG parameters used are showed in the appendix. To evaluate the proposed algorithm, computer simulations have been conducted using MATLAB.

The controlled WECS performances depend on the wind speed variations. So, to analyze the performances of the proposed SS_DTC under SMRFO, the effect of three different wind profiles is investigated in this section:

Case *A*: we consider linear variations of the wind speed as expressed in the following equations:

$$V_V = \begin{cases} 8.5t + 4.5 \ for & 0 \le t < 1 \\ 13 \ for & 1 \le t < 2 \\ -6t + 25 \ for & 2 \le t < 3 \\ 7 \ for & 3 \le t < 4 \\ 10t - 33 \ for & 4 \le t < 5 \\ 17 \ for & t \ge 5 \end{cases} \quad (27)$$

Case *B*: Non linear wind speed variations at low frequency are applied. The wind is expressed as:

$$V_V = 10 + \sin(\omega_V) - 0.875\sin(3\omega_V) + 0.75\sin(5\omega_V) - 0.625\sin(10\omega_V) + 0.5\sin(30\omega_V) + 0.25\sin(50\omega_V) + 0.125\sin(100\omega_V) \quad (28)$$

With: $\omega_V = 2\pi/10$

Case *C*: A fluctuated wind speed at high frequency is used in this test as expressed in the following equation:

$$V_V = 10 + \text{rand}\left(1 - 0.05\cos\left(\frac{2\pi t}{20}\right) - 0.05\cos\left(\frac{2\pi t}{600}\right)\right) \quad (29)$$

Figure (8) shows the real, observed and reference speed, and the real and observed speed errors for each case. For these three cases, real and observed speeds converge to their reference values in a very short time. The maximum values errors computed are equal to *8%*. The maximum value is found at the moment of speed jump.

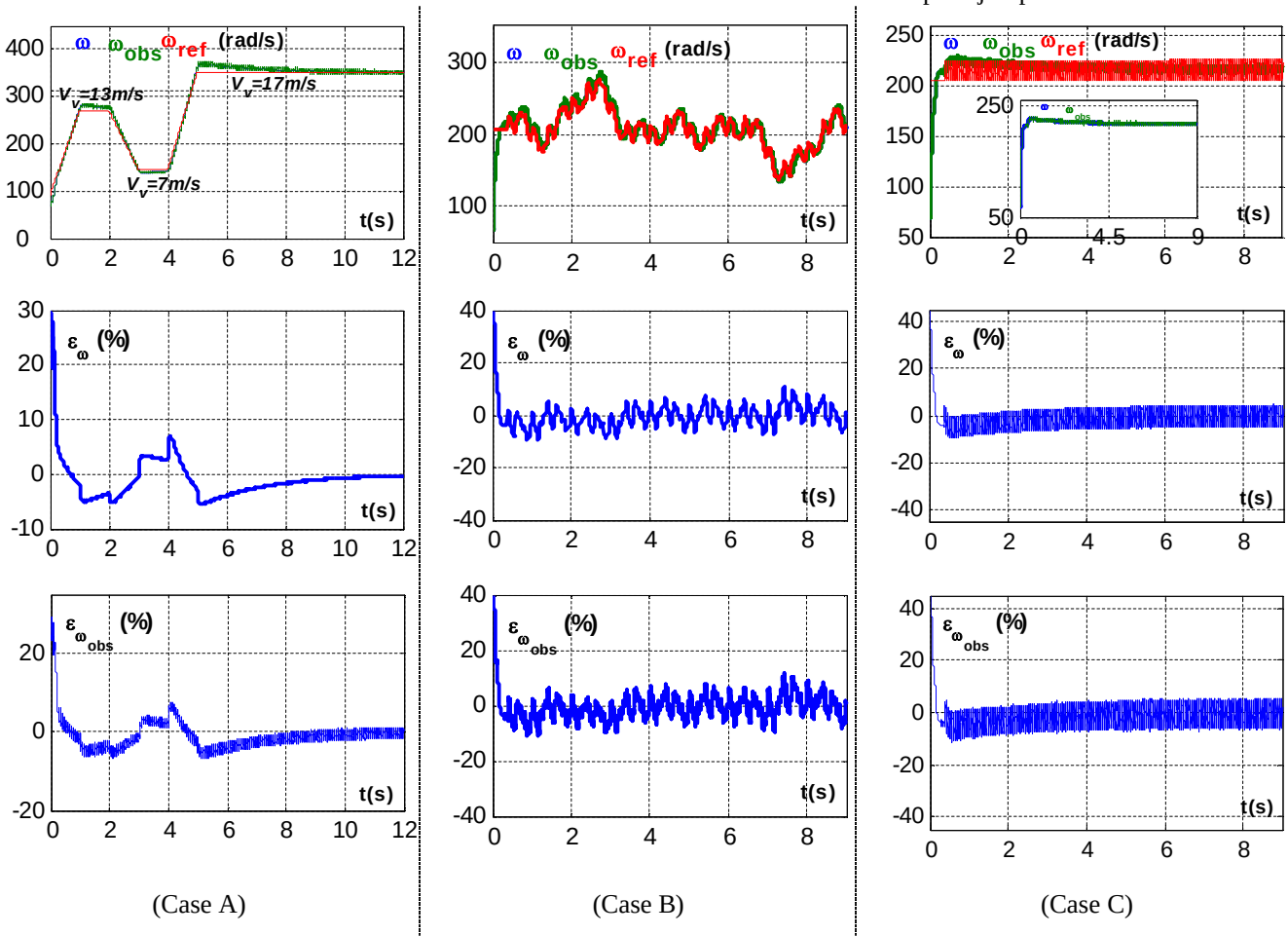

(Case A) (Case B) (Case C)

Fig. 8. The real, observed and reference speed, the real speed estimation error and the observed speed estimation error for: Case A: lineare wind variation, Case B: low frequency wind variation,Case C: hight frequency wind variation

As shown in figure (9), in case A one may remark that the wind variation has influence on the location of system operation mode. The stator and the GSC output active powers show that, for sudden wind variations, the WECS switches between the subsynchronous generating mode, hypersynchronous speed mode and motoring mode as seen in table 2.

Table 2. WECS operating mode for linear wind variations

Generating mode Sub. ($\omega<\omega_s$)	Motoring mode	Generating mode Hyper. ($\omega>\omega_s$)
$P_s<0$	$P_s>0$	$P_s<0$
$P_g>0$	$P_g>0$ *or* $P_g<0$	$P_g<0$
$T_{em}<0$	$T_{em}>0$	$T_{em}<0$

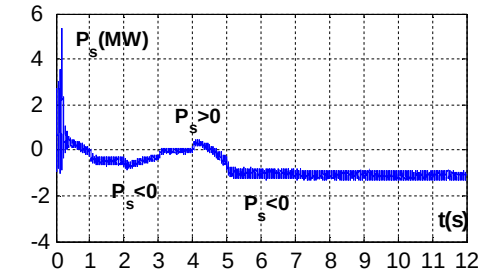

(a)

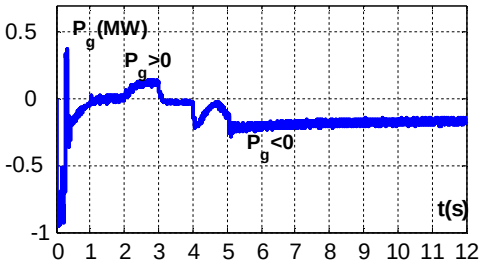

(b)

Fig. 9. Injected active power during the test in case(A): (a) in the stator side, (b) in the GSC

In order to test the robustness of the proposed observer and the system performances, we have simulated the system under rotor and stator resistances variations. Firstly, the rotor resistance increases by 50% of the nominal value, from t=1.4s to 1.6s. Secondly, from t=1.8s to 2s the stator resistance increases by 50% of the nominal value. Figure (10) illustrates the real and the observed rotor flux while figure (11) illustrates the magnitude of stator flux, the stator current error and the Stator Power factor (SPF). As it may be observed, the proposed approach allows a quick flux response to be achieved. Stator flux and stator current errors are evaluated respectively at 1% and 3%.

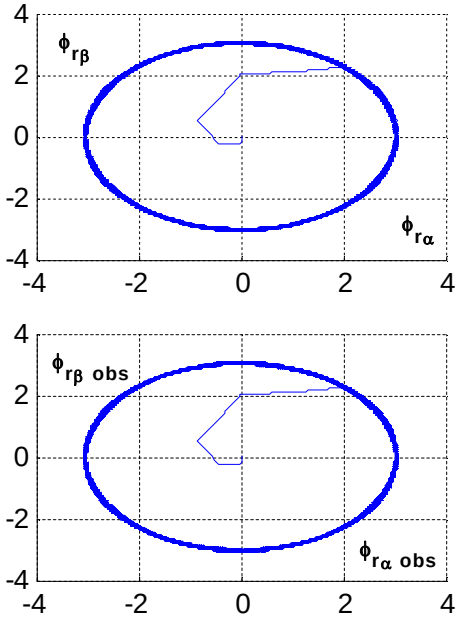

Fig. 10. The real and observed rotor flux magnitude

The proposed SMRFO show a very high fidelity and robustness against parameter variations. These are verified by the convergence of sliding surfaces to zero. The stator is directly connected to the grid, so the stator flux converges to its reference value about t=0.7s. SPF variations converge to -1, this confirms the null-VAR operation mode.

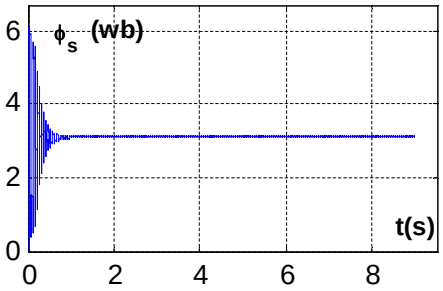

(a)

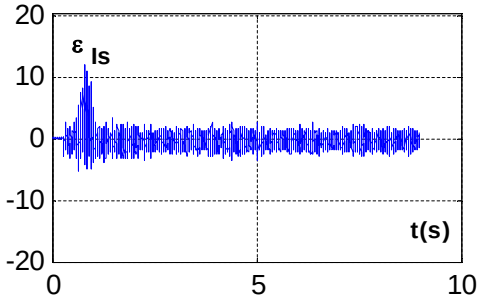

(b)

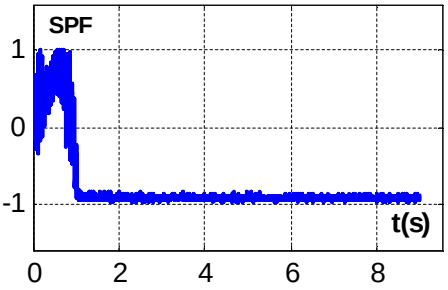

(c)

Fig. 11. Stator performances: (a) The real stator flux magnitude, (b) the stator current estimated error,(c) The stator power factor

Figure (12) illustrate the grid performances which confirm, as in the previous simulation, the efficiency of the MPPT, the SS_DTC and the NVVOC strategies. The transient's active and reactive powers are controlled perfectly. The currents and the voltages in the three phase's network constitute a balanced system of the rural network frequency.

7. Conclusion

In this paper a WECS based on a DFIG is presented. The DFIG model has been associated with a wind turbine one operated in MPPT mode. The system uses two rotor power converters linked by a DC bus which achieve control of

active and reactive powers exchanged between the local grid and the system. The SS_DTC is applied to the RSC and the NVVOC strategy is applied to the GSC. The introduction of the SMRFO allows an easier rotor flux regulation and shows an increase of efficiency and a high dynamic performance.

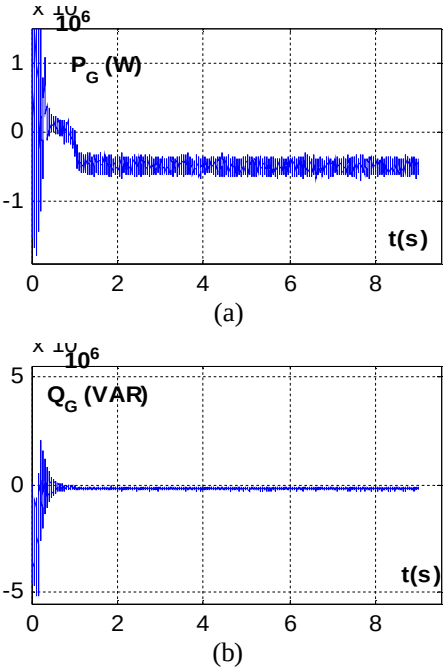

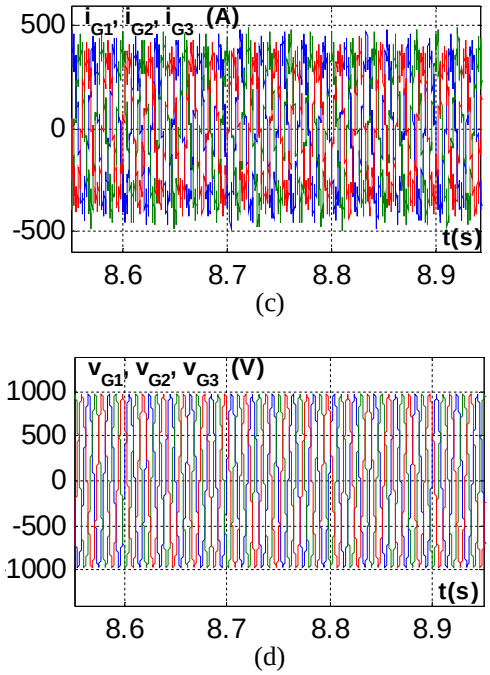

Fig. 12. Grid performances: (a) the real power injected, (b) the reactive power injected, (c) the three phase grid currents (zoom), (d) the three phase grid voltages (zoom)

Appendix

Induction generator data
Rated power: *660 Kw,*
Rated stator voltage: *400/690V, 50Hz,*
R_r*=0.0238* Ω, R_s*=0.0146* Ω,
L_s*=0.0306 H,* L_r*=0.0303H, M=0.0299H,*
J_m*=28 kg.m*^{2}, Number of pair poles: n_p*=2,*
Damping coefficient: *f =26*

Power coefficient expression

$$C_p = \sum_{i=0}^{5} a_i \lambda^i$$

With:
a_5*=-0.000373,* a_4*=0.009309,*
a_3*=-0.081857,* a_2*=0.2774,*
a_1*=-0.19084,* a_0*=0.021945.*

Wind turbine data
Number of blades=3,
Rotor diameter: $2R_b$*=43.5m,*
Gearbox coefficient: *m= 55,*
Cut-in wind speed: V_{min}*=3m/s,*
Cutoff wind speed: V_{max}*=25m/s,*
Optimal tip speed ratio*:* λ_{opt}*=4,*
Moment of inertia: *J=238 kg.m*^{2}.

Grid data
Network rated voltage: v_R*=975V, 50Hz,*
R_L*=3*Ω *,*
L_L*=0.051H*

Nomenclature

General		*Subscripts*	
i	Instantaneous current *(A)*.	*t*	Turbine.
v	Instantaneous voltage *(V)*.	*s, r*	Stator and rotor.
T	Torque *(Nm)*.	*m*	Mechanic
J, f	Inertia and viscous friction.	*g*	Output grid side converter
φ	Flux linkage vector *(Wb)*.	*G*	Grid
ω	Angular speed of the rotating field *(rad/s)*.	*L*	Line
θ	Angle	*a,b,c*	Quantities in *a,b and c*-axis
R	Resistance *(Ω)*.	*α,β*	Quantities in *α*-axis and *β*-axis
M	Magnetizing inductance.	dc	dc link.
L	Total cyclic inductance	*ref*	Reference value.
σ	Leakage factor, $\sigma = 1 - \frac{M^2}{L_S L_r}$	e	Estimated value.
X, Y	State and output vector.	*Superscripts*	
V_v	Wind speed *(m/s)*.	*	Conjugate
P, Q	Active, Reactive power	*s*	Stationary reference frame
		r	Rotor reference frame

References

[1] Wei Qiao, R.G. Harley. Improved Control of DFIG Wind Turbines for Operation with Unbalanced Network Voltages. 'IAS08 Annual Meeting. IEEE . pp.1 -7. October 2008.

[2] D. Casadei, F. Profumo, G. Serra, A. Tani. FOC and DTC: Two viable schemes for induction motors torque control. IEEE Trans. Power Electron. Vol.17. no.5, pp.779-787. September 2002.

[3] A. Tapia, G. Tapia, J.X. Ostolaza, J.R. Saenz, Modeling and control of a wind turbine driven doubly fed induction generator. IEEE Trans. Energy Conversion. Vol. 18, Issue 2, pp. 194 - 204. June 2003.

[4] C. Belfedal, S.Moreau, G.Champenois, T.Allaoui, M.Denai. Comparison of PI and Direct Power Control with SVM of Doubly Fed Induction Generator. Journal of Electrical and Electronics Engineering. Vol. 8, no.2. pp.633-641. 2008.

[5] J. Ben Alaya, A. Khedher, M.F. Mimouni. Variable Speed Vector Control Strategy of the Double Fed Induction Generator Integrated in Electrical Grid. Inter. Conf. on Ecologic Vehicles and Renewable Energy (EVER'08), Monaco, France. March 2008.

[6] J. Ben Alaya, A. Khedher, M.F. Mimouni. Nonlinear Vector Control Strategy Applied to a Variable Speed DFIG Generation System, IEEE 8th International Multi-Conference on Systems, Signals and Devices,.SSD'2011

[7] Wong, K.C., Ho, S.L., Cheng, K.W.E., Direct control algorithm for doubly fed induction generators in weak grids. Electric Power Applications, IET. Vol. 3, Issue 4, pp. 371 - 380, July 2009.

[8] M. Rahimi, M. Parniani. Dynamic behavior analysis of doubly-fed induction generator wind turbines, The influence of rotor and speed controller parameters. Int. J. of Electrical Power and Energy Systems. Vol.32, Issue 5, pp. 464-477, 2010.

[9] F. Bonnet, P.E. Vidal, M. Pietrzak-David. Dual Direct Torque Control of Doubly Fed Induction Machine. IEEE Trans. Industrial Electronics. Vol. 54, no.5, pp. 2482-2490. October 2007.

[10] G. Abad, M. A. Rodríguez, J. Poza. Two-Level VSC Based Predictive Direct Torque Control of the Doubly Fed Induction Machine With Reduced Torque and Flux Ripples at Low Constant Switching Frequency. IEEE Trans. Power Electronics. Vol.23. Issue 3, pp. 1050-1061. May 2008.

[11] F. Parasiliti, R. Petrella, M. Tursini. Adaptive sliding mode observer for speed sensorless control of induction motors. 34th IAS Annual Meeting, IEEE. pp.2277-2283. 1999.

[12] A. Khedher, M.F. Mimouni, A. Masmoudi, N. Derbel. Robust field Oriented Control analysis of an induction motor using an adaptive flux observer based on sliding mode methodology. IEEE. MESM'2004. pp.184-190. Sharjah, UAE. January 2004.

[13] Dimitrios G Giaourakis, Athanasios N Safacas, Savvas N Tsotoulidis, "Dynamic Behaviour of a Wind Energy Conversion System including Doubly-Fed Induction Generator in Fault Conditions", International Journal of Renewable Energy Research (IJRER), Vol. 2, No. 2, pp. 219-226, 2012.

[14] Hicham Serhoud, Djilani Benattous, "Maximal Wind Energy Tracing of Brushless Doubly-Fed Generator under Flux Oriented Vector Control", International Journal of Renewable Energy Research (IJRER), Vol. 2, No. 2, pp. 236-242, 2012.

[15] A. K. Azad, M. Masud Kaysar, "Design of a Horizontal Axis Wind Turbine for Electricity Generation in Low Speed Windy Sites"" International Journal Of Advanced Renewable Energy Research, Vol. 1, Issue. 6, pp. 363- 373, 2012.

[16] I. Takahashi, T. Nouuchi. A new quick-response and high-efficiency control strategy of an induction motor. IEEE Trans. Ind. Appl. Vol. IA-22, No. 5, pp. 820-827. September/October 1986.

[17] F. Z. Peng, T. Fukao. Robust speed identification for speed-sensorless vector control of induction motors. IEEE Trans. Ind. Appl., vol. 30, No. 5, pp. 1234-1240, September./October 1994.

[18] C. Schauder. Adaptive speed identification for vector control of induction motors without rotational transducers. IEEE Trans. Ind. Appl., Vol.28, No. 5, pp. 1054-1061, September/October 1992.

[19] L. Morel, H. Godfroid, A. Mirzoian, J.M. Kauffmann. Doubly-fed induction machine: converter optimization and field orientation control without position sensor. Proc. IEE, Vol. EPA - 145. No. 4. pp. 360 - 368. 1998.